Title
Simpler and Faster: An Improved Heat Index

Journal
Journal of Applied Meteorology and Climatology, 65(5)

ISSN
1558-8424

Authors
Lu, Yi-Chuan
Goodman, Alex
Kalmus, Peter
et al.

Publication Date
2026-05-01

DOI
10.1175/jamc-d-25-0067.1

Simpler and faster: an improved heat index

Yi-Chuan Lu,[a,b] Alex Goodman,[c] Peter Kalmus,[c] and David M. Romps[a,b]

[a] *Department of Earth and Planetary Science, University of California, Berkeley, California, USA*
[b] *Climate and Ecosystem Sciences Division, Lawrence Berkeley National Laboratory, Berkeley, California, USA*
[c] *Jet Propulsion Laboratory, California Institute of Technology, Pasadena, California, USA*

ABSTRACT: The existing heat index is complicated and slow. Furthermore, its complexity has obfuscated both mathematical inconsistencies (double values) and physical inconsistencies (supersaturation). This paper presents a simplified heat index that resolves these issues. The new approach results in small changes to the heat index for air temperatures below 300 K, but leaves the heat index unchanged for air temperatures above 300 K, where it is most commonly used. This simplification enhances interpretability, and a refactored algorithm accelerates the computation of the heat index by orders of magnitude. The optimized implementation is freely available in C++, R, and Python. In this article, we also clarify a long-standing ambiguity regarding "compensable" and "uncompensable" heat stress. Historically, "uncompensable" denoted conditions leading to fatal core temperatures. Recent studies, however, have applied the term to any inflection followed by a rise in core temperature. Using the heat index model, we show that such an observation does not necessarily imply lethality, because heat loss increases with core temperature and can yield a stable, non-fatal equilibrium. To avoid ambiguity, we therefore replace compensable/uncompensable with normothermic, hyperthermic, and lethal categories based on the predicted steady-state core temperature.

SIGNIFICANCE STATEMENT: Despite the wide use of the heat index in meteorology and climate science, the thermoregulatory model underlying the heat index is not widely known or understood, likely due to its complexity. In this article, we simplify the model at low temperatures (<300 K) and present a graphical method for calculating the heat index, making its structure more intuitive. Additionally, we provide an implementation of the heat index in a low-level programming language, enabling efficient computation of the heat index for various applications.

1. Introduction

The heat index is widely used by both weather forecasters and climate scientists, but the algorithm for calculating it is complex, slow to compute, and, as will be shown here, double-valued. In its original formulation by Steadman (1979, hereafter S79), the heat index had the additional problem of being defined for only a narrow range of temperatures. The "narrow range" problem was fixed by Lu and Romps (2022, hereafter LR22), who extended the calculation of the heat index to all combinations of temperature and humidity, but the other problems remained. In fact, as shown here, the algorithm of LR22 introduced a new problem: supersaturated skin and clothing at cold temperatures.

Here, we will address all of these issues. The double values, supersaturation, and model complexity all stem from the inclusion of clothing as a separate layer in the heat and moisture budgets. Therefore, we will simplify the heat index by eliminating the clothing as a separate layer. This simplification eliminates the double values and supersaturation, and it dramatically reduces the model's complexity. To address the speed of computation, it is worth noting that the only publicly available code for computing the heat index from Steadman's equations (released by LR22) relies on doubly nested root solvers. Refactoring the algorithm eliminates that nesting. What results is a simpler and faster heat index. Given tabulated solutions to those equations, polynomial equations can be used to approximate the heat index, yielding answers even more quickly (Rothfusz 1990; Lanzante 2024). See, however, Romps and Lu (2022) for a discussion of the limitations of the approximation by Rothfusz (1990). For a more detailed discussion of computational speed, see Section 6.

Fortunately, the simplification does not affect the heat index where it matters the most. The values of the heat index and their physiological implications are unaltered for air temperatures above 300 K (27 °C or 81 °F). Therefore, previous results using the extended heat index of LR22 at high temperatures are unaffected, including the finding that the National Weather Service has underestimated the heat index during severe heat waves (Romps and Lu 2022), or that the heat index can predict the onset of hyperthermia in human-subject experiments (Lu and Romps 2023b), and that unabated anthropogenic climate change would subject wide swaths of Earth to conditions that are hyperthermic and even lethal

Corresponding author: Yi-Chuan Lu, yclu@berkeley.edu

(Lu and Romps 2023a). Furthermore, the refactored algorithm dramatically accelerates computations, facilitating the calculation of the heat index on large volumes of weather and climate data.

2. History

The heat index was first introduced in S79 by Robert Steadman, who called it the "apparent temperature" before it later became known as the heat index. By definition, the heat index is the air temperature at a reference vapor pressure of 1.6 kPa that would induce the same behavioral and physiological response as the actual air temperature and humidity. For succinctness, we will use the word physiology to refer to both behavior and physiology. Given assumptions about, e.g., the wind speed and the size, activity, and sun exposure of a human, that human's physiological state is a function of the air temperature and relative humidity. Therefore, the definition of the heat index HI can be expressed mathematically as

$$\text{physiology}\left(\text{HI}, \frac{1.6\text{ kPa}}{p^*(\text{HI})}\right) = \text{physiology}(T_a, \text{RH})\,, \tag{1}$$

where "physiology" in this equation is a function that returns the physiological state, T_a is the air temperature, RH is the relative humidity, and p^* is the saturation vapor pressure as a function of air temperature. Note that the expression $1.6\text{ kPa}/p^*(\text{HI})$ is the relative humidity corresponding to a vapor pressure of 1.6 kPa when the air temperature equals HI. Therefore, equation (1) says that the state induced by an air temperature of HI and a vapor pressure of 1.6 kPa is the same as the state induced by the actual T_a and RH.

Note that equation 1 makes no assumptions about the underlying human. The human could be resting or walking, exposed to sunlight or shade, healthy or ill. However, those assumptions do affect the functional form of the "physiology" function. Specifically, S79 defined the "physiology" function by assuming a young, healthy adult walking in the shade (corresponding to a metabolic rate per skin area of 180 W m^{-2}) while exposed to a wind of 1.5 m s^{-1}. Furthermore, the human is assumed to exhibit some idealized behaviors, such as removing clothing as needed to maximize cooling. Therefore, if this idealized human experiences a given heat stress, any real person would experience that stress level or higher.

Using these assumptions and equation (1), S79 tabulated, in his Table 2, values of the heat index for every 1 °C of air temperature and every 10% of relative humidity. Unfortunately, the physiological model of S79 was defined only within a limited temperature range. For example, at 50% relative humidity, the heat index was defined only up to 37 °C (99 °F). At 100% relative humidity, the heat index was defined only up to 27 °C (81 °F). The regions where S79 had defined the heat index are labeled by III and IV in Figure 1a. S79 gave some values in parentheses at slightly higher temperatures in his Table 2, but those were extrapolations into an unphysical physiological state with supersaturated skin. S79 acknowledged this limitation and largely refrained from tabulating the heat index beyond where the model was physical.

After its introduction in 1979, the heat index was soon adopted by the United States National Weather Service (NWS). Since the code for calculating the heat index was not widely available[1], and since interpolation of tabulated values was unwieldy, Rothfusz (1990) fit a polynomial (in temperature and relative humidity) to Table 2 of S79. Unfortunately, this allowed the NWS and others to extrapolate beyond the values calculated by S79, leading to the communication of heat index values with no scientific basis.

The orange wedge in Figure 1a shows the range of air temperatures and relative humidities covered by the NWS heat index chart, which presents values calculated using the Rothfusz (1990) polynomial[2]. In that NWS chart, the heat index is extrapolated to air temperatures that are 3-5 °C beyond where the heat index model of S79 had been defined. As shown in Figure 10 of LR22, the values in the current NWS table of heat index values are in error by as much as 16 °C (28 °F).

[1]We are not aware of anyone other than Steadman having coded up the heat index's underlying physiological model, although Steadman sold a version of the algorithm in Excel in later years (personal communication with Robert Steadman in October of 2022, the month before he passed).

[2]E.g., https://www.weather.gov/safety/heat-index, https://www.weather.gov/ama/heatindex, and https://www.weather.gov/ffc/hichart, as accessed on March 8, 2025

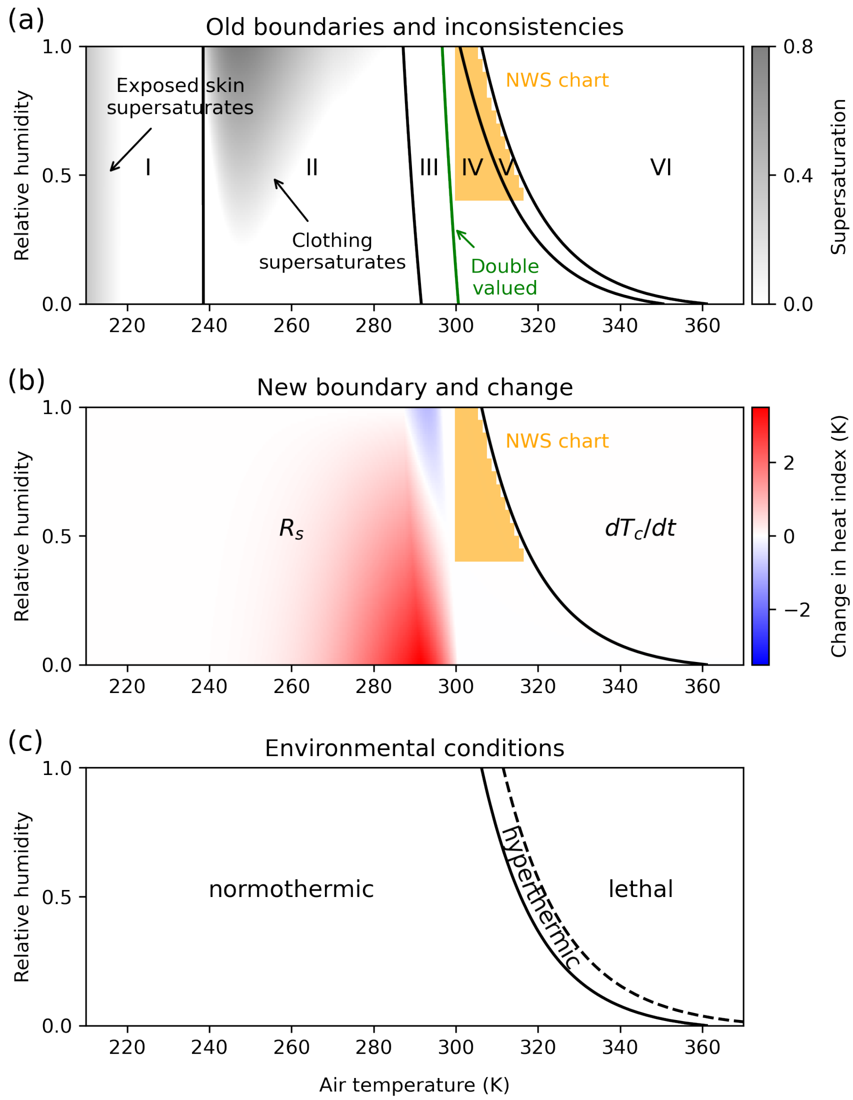

FIG. 1: (a) Six regions (I–VI) in the temperature-humidity space defined by LR22. S79 defined the heat index in regions III and IV, and LR22 extended the heat index into regions I, II, V, and VI. The orange wedge indicates the region where the National Weather Service tabulates heat index values using the polynomial by Rothfusz (1990). The small region between III and IV, where the heat index is double-valued, is shown as a green curve. The grey heat map shows the level of supersaturation at the exterior surfaces of clothing and exposed skin. (b) In the simplified heat index, the shell's thermal resistance R_s varies in a subset of T_a-RH space and the core's temperature tendency dT_c/dt varies in the complement. The boundary between those two subsets is identical to the boundary between V and VI in panel (a). The heat map shows the changes in the heat index due to the simplification. Red indicates where the new, simplified heat index gives higher values than the original, and blue indicates where the new values are lower. The change is zero in regions IV, V, and VI by construction and the maximum change of 3.5 K occurs in region III. The change is identically zero for all air temperatures above 300.6 K. (c) The boundaries of normothermic, hyperthermic, and lethal environmental conditions for both LR22 and this article.

S79 defined the heat index only within the regions labeled III and IV in Figure 1a. LR22 extended the heat index to all regions I through VI. To extend the heat index into regions V and VI, there was only one natural solution to the supersaturation problem encountered by S79, and that was to let excess sweat drip off the skin (LR22). The distinction between regions V and VI is that region V is where the core temperature can still be maintained at its normal value and region VI is where hyperthermia is unavoidable.

3. Inconsistencies

In S79 and LR22, region III is distinguished from region IV by the inclusion of clothing, which adds considerable complexity to the model. In fact, as we have discovered, that complexity generates and obfuscates a fundamental problem: the heat index is double-valued at the transition between regions III and IV. The root cause of this is that S79 was unable to join regions III and IV at a one-dimensional curve in T_a-RH space. Instead, S79 defined regions III and IV such that they overlap in a thin two-dimensional subset of T_a-RH space. This causes the "physiology" function to be double-valued there and, consequently, the heat index defined by equation (1) is double-valued there as well.

The two-dimensional subset where regions III and IV overlap is drawn in green in Figure 1, where it appears to be one-dimensional due to how thin it is; see Appendix A for a zoomed-in view. In practice, the width of the green region is less than 0.04 K, and the difference between the two possible heat index values is less than 0.03 K. Nevertheless, the heat index is intended to be a function of environmental conditions, so any multiplicity of possible values is a fundamental flaw. Furthermore, LR22 was unaware of this double-valued problem, so it persisted in their algorithms as well: the R, Python, and Fortran codes released along with LR22 handled the double-value problem using different implementations and gave different bad results; see Appendix A for details.

To the left of region III in Figure 1a, S79 did not define the heat index because the vapor pressure used for the reference state (1.6 kPa) exceeds the saturation vapor pressure (i.e., another problem with supersaturation). The fix introduced by LR22 was to simply define the reference vapor pressure as the lower of 1.6 kPa and the saturation vapor pressure. In other words, LR22 extended the heat index into region II by replacing equation (1) with

$$\text{physiology}\left(\text{HI}, \min\left(\frac{1.6\ \text{kPa}}{p^*(\text{HI})}, 1\right)\right) = \text{physiology}(T_a, \text{RH})\,. \tag{2}$$

By S79's convention, the layer of clothing covers 84% of the skin. At the cold edge of region II, the clothing must be perfectly resistant to the flow of heat and moisture to allow the human to maintain a normal core temperature. To extend the heat index into region I, LR22 allowed the coverage of that clothing to increase beyond 84%. Unknown to LR22 at the time, these straightforward extensions of S79's model into regions II and I can generate an unphysical supersaturation of the clothing (in region II) and exposed skin (in region I). The level of supersaturation is shown as shaded grey areas in Figure 1a. Here, supersaturation is defined as the relative humidity minus one. For example, a supersaturation of 0.4 implies the vapor pressure is 1.4 times the saturation vapor pressure.

We see, therefore, that the existing heat index suffers from both mathematical and physical inconsistencies. These inconsistencies have gone unnoticed until now in part because of the considerable complexity of the underlying physiological model: in the original model of S79, there are seven nonlinear equations that must be solved for seven unknowns. Beyond concealing inconsistencies, this complexity has also posed an unnecessary barrier to the comprehension and application of the heat index.

4. Simpler

In the model of S79 and LR22, the thin slice of T_a-RH space where the heat index is unintentionally double-valued (the green curve in Figure 1a) lies at the boundary between a simple two-component model of thermoregulation (regions IV-VI) and a complicated four-component model (regions I-III). In the latter, those four components are the core, exposed skin, clothed skin, and clothing. In the simplification presented here, we eliminate the clothing as a *separate* layer and, instead, fold the effects of clothing into a more general layer that we call the **shell**. Thus, in the unclothed regions (IV-VI), the shell is simply exposed skin, whereas, in the clothed regions (I-III), the shell will represent the combined effects of skin and clothing.

Note that this simplification leaves the heat index in regions IV, V, and VI unaltered. This means that the simplified heat index described here is backwards compatible with all previously valid heat index values reported in air temperatures above 300 K (27 °C or 81 °F). Note, for example, that the NWS heat index chart lies entirely within regions IV and V, so the corrected NWS chart presented in Figure 10 of LR22 is not affected.

With this simplified heat index, there is no longer a need for six regions. With respect to the algorithm, we may think of T_a-RH space as being divided into two subsets: conditions in which the physiological state is described by the thermal resistance R_s of the shell, and conditions in which the physiological state is described by the tendency of the core temperature dT_c/dt at an initial core temperature of 310 K. The boundary between these two subsets is shown by the black curve in Figure 1b. This boundary is identical to that between regions V and VI in Figure 1a. In Figure 1b, we also show the change in the heat index value after we use this "shell" model. The changes are minor, with red indicating where the new heat index is greater than the old, and blue indicating where it is less than. The change is zero in regions IV-VI by construction and the maximum change of 3.5 K occurs in region III. Above a temperature of 300.6 K, the changes are identically zero for all values of relative humidity.

With respect to physiological outcomes, we may divide the space into three regions as shown in Figure 1c. The normothermic region, which encompasses the old regions I-V, corresponds to all conditions for which the core temperature can be maintained at a normal value of 310 K (37 °C or 98.6 °F). Normothermia is achieved by tuning the resistance of the shell to heat and moisture by modulating skin blood flow and, as needed, the thickness of clothing[3]. The hyperthermic region, which encompasses a part of the old region VI, is where no amount of skin blood flow or sweat can maintain the core at a temperature of 310 K, but for which the steady-state core temperature is less than 315 K. See section 5a for a discussion of the relationship between instantaneous dT_c/dt and the steady state T_c. Finally, the lethal region is that part of the old region VI for which dT_c/dt would still be positive at $T_c = 315$ K.

In the normothermic region, we use equations (14-16) of LR22, previously used only in regions IV and V. Those equations are

$$0 = Q - Q_v - \frac{T_c - T_s}{R_s}, \tag{3}$$

$$0 = \frac{T_c - T_s}{R_s} - \frac{T_s - T_a}{R_a} - \frac{p_s - p_a}{Z_a}, \tag{4}$$

$$p_s = \min\left[\frac{Z_s p_a + Z_a p_c}{Z_s + Z_a}, \phi_{\text{salt}} p^*(T_s)\right], \tag{5}$$

where T_c, T_s, and T_a are the temperatures of the core, shell, and air; p_c, p_s, and p_a are the vapor pressures of the core, shell, and air; ϕ_{salt} is the effective relative humidity of sweat; p^* is the saturation vapor pressure; R_s and R_a are the resistance to heat flow through the shell and air; Z_s and Z_a are the resistance to mass (i.e., sweat) flow through the shell and air; Q is the metabolic heat flux generated in the core; and Q_v is the respiratory heat flux from the core to the air.

These equations describe a steady-state solution to thermoregulation with a normothermic core temperature of $T_c = 310$ K. The first equation describes the core's heat balance, which has metabolic heat production Q balanced by ventilation Q_v and the flow of heat from core to shell. The second equation describes the heat balance of the shell, which is affected by the flow of heat from core to shell, the flow of heat from shell to air, and the cooling from evaporation of sweat. The third equation is the solution for the vapor pressure of the partially wetted shell. The minimum function was introduced by LR22 and ensures that the vapor pressure does not exceed the saturation vapor pressure of sweat; in effect, this allows excess sweat to drip off the shell.

With the addition of some other constraints laid out in LR22 (e.g., $T_c = 310$ K), these three equations have three unknowns: T_s, p_s, and R_s. Using equations (3) and (5) to eliminate T_s and p_s from equation (4), we are left with a single equation in a single unknown, which is the shell's resistance to heat R_s. The value of R_s defines the physiological state, which can be interpreted in terms of skin blood flow in the old regions IV and V and as the combined effect of skin and clothing in the old regions I, II, and III.

In of LR22's use of equations (3–5), R_s is between 0 to 0.0387 m^2 K W^{-1}, with 0 occurring at the hot end of region V and 0.0387 m^2 K W^{-1} occurring at the cold end of region IV. The simplification we introduce here is to extend (3–5) into regions I, II, and III, allowing R_s to exceed 0.0387 m^2 K W^{-1} when transitioning into region III. At the same time, R_s now represents the thermal resistance of the shell, which can represent the combined effects of tissue conductance, skin blood flow, and also clothing. Mathematically, this continuation of (3–5) to colder temperatures is straightforward, and it does not generate any supersaturation of the shell.

For the hyperthermic and lethal regions, we use equation (18) of LR22. That equation is

$$C_c \frac{dT_c}{dt} = Q - Q_v - \frac{T_c - T_a}{R_a} - \frac{p_c - p_a}{Z_a}, \tag{6}$$

where C_c represents the heat capacity of the core. In these regions, R_s is zero, meaning the body's skin blood flow has brought the skin temperature all the way to the core temperature, and so the body has exhausted all physiological

[3]Note that the heat index uses a passive model of physiology, so elevated sweating and skin blood flow are triggered without a rise in core temperature. For an active model, in which those responses are functions of the core temperature, it would be appropriate to define normothermic conditions as those that generate a core temperature close to 310 K, e.g., below 311 K.

mechanisms available to control T_c. Therefore, the physiological state in the hyperthermic and lethal regions is described by dT_c/dt at the initial core temperature of $T_c = 310$ K. Equation (6) gives dT_c/dt in terms of the metabolic heat production, respiratory heat loss, and the flow of sensible and latent heat from the body to the air. Although dT_c/dt is all that is needed to define the physiological state and the heat index, equation 6 can be solved to determine the evolution of T_c as a function of time, and we will take advantage of that in the next section.

5. Interpretation

In the following subsections, we will discuss how to interpret the states predicted by this simplified model of physiology. In particular, we will explain the advantages of using the terms normothermic, hyperthermic, and lethal instead of the popular, but ambiguous, terms of compensable and uncompensable (section 5a). We will then show that the heat index *values* are simply a convention for ranking and labeling the states predicted by the underlying physiological model (section 5b). Finally, we will interpret the heat index's physiological states in terms of quantities relevant to an assessment of heat stress, such as skin blood flow, equilibrium core temperature, and the time it takes to reach a lethal core temperature (section 5c).

a. Normothermic, hyperthermic, and lethal

Over many decades, it has been common practice to partition environmental conditions into two categories: compensable and uncompensable (e.g., Taylor 1957; Webb 1959; Nunneley 1970; Webb 1975; Kraning and Gonzalez 1991; Cheung et al. 2000; Foster et al. 2020; Cramer et al. 2022; Wolf et al. 2022; Cottle et al. 2022). In many of these studies, uncompensable is defined as "a continuous rise in T_c" or "a state where the rate of heat storage is positive." However, strictly adhering to this definition encompasses scenarios that are manifestly survivable. For example, a core temperature T_c that, for times $t \geq 0$, satisfies $T_c = 311\ \text{K} - (1\ \text{K}) \exp[-t/(1\ \text{hr})]$ will rise continuously and nonstop for all time, but it never exceeds 311 K. It is unlikely that the physiological literature intends to classify such mild hyperthermia as "uncompensable." Therefore, one interpretation is that the intended meaning of "uncompensable"—even if unstated—is that T_c would continue rising until death. We adopt this definition here: compensable conditions are those where the human body can attain a steady-state thermal balance at survivable T_c (even if hyperthermic), whereas uncompensable conditions are those that will generate, with sustained exposure, a fatal core temperature.

Recently, many physiology experiments have claimed that conditions are uncompensable merely by observing an inflection point followed by a rising T_c (Wolf et al. 2022; Cottle et al. 2022). However, this observation alone does not guarantee the rise will persist until death. Instead, given a functioning thermoregulatory system, the body's gross export of heat *increases* as the body warms, which can lead to a thermal steady state well before a lethal core temperature is reached. That increase in gross heat export occurs primarily because the skin, which is closely pegged to the core temperature in a hyperthermic state, sheds sensible and latent heat faster the warmer the core gets. Additional contributions to export are made from an increased export of sensible and latent heat via ventilation (i.e., from the lungs) and from an increased emission of longwave radiation. These effects manifest in equation (6) as an increase in T_c, p_c, and Q_v (corresponding to increased export of sensible and latent heat) and a decrease in R_a (corresponding to an increase in longwave emission; see LR22 for details), all of which tend to drive dT_c/dt back towards zero.[4]

To demonstrate this behavior, Figure 2a shows a time series of T_c generated by integrating equation 6 with an initial condition of $T_c = 310$ K at $t = 0$ under the condition of $(T_a, \text{RH}) = (310\ \text{K}, 1)$. For this air temperature and humidity, the core temperature equilibrates at 313.5 K, as indicated by the horizontal grey dashed line. Note that the slope of the curve dT_c/dt at $t = 0$ is about 0.12 °C per minute (7.4 °C per hour). That heating rate is an order of magnitude larger than heating rates identified as "uncompensable" in laboratory experiments (Cottle et al. 2022; Wolf et al. 2022). We see in this example, however, that T_c plateaus at a hyperthermic but non-lethal steady state, which tells us the conditions are compensable.

Note that the time scale for approaching equilibrium depends on the wind speed: a lower wind speed would bring the body to equilibrium more slowly. For example, in Figure 2a, the time scale for T_c to reach equilibrium is about 2 hours. By contrast, using a seated metabolic rate of 58 W m^{-2} (Parsons 2014) and a much lower wind speed of 0.2 m s^{-1} — a typical value found in climate chamber experiments (Lu and Romps 2023b) — yields a similar equilibrium

---

[4]Some physiology models (e.g., Ravanelli et al. 2019; Vanos et al. 2023; Fan and McColl 2024; Guzman-Echavarria et al. 2024) impose a fixed skin temperature. As a result, once the system falls out of heat balance, because increases in the sweating rate yield no additional evaporative cooling, it remains out of balance and T_c rises continuously until death. In this respect, these models represent an unphysical system, allowing the core temperature to rise, but not the skin temperature. This behavior contradicts laboratory findings showing that skin temperature increases alongside core temperature once hyperthermia is reached (Ravanelli et al. 2017; Vecellio et al. 2022; Meade et al. 2025).

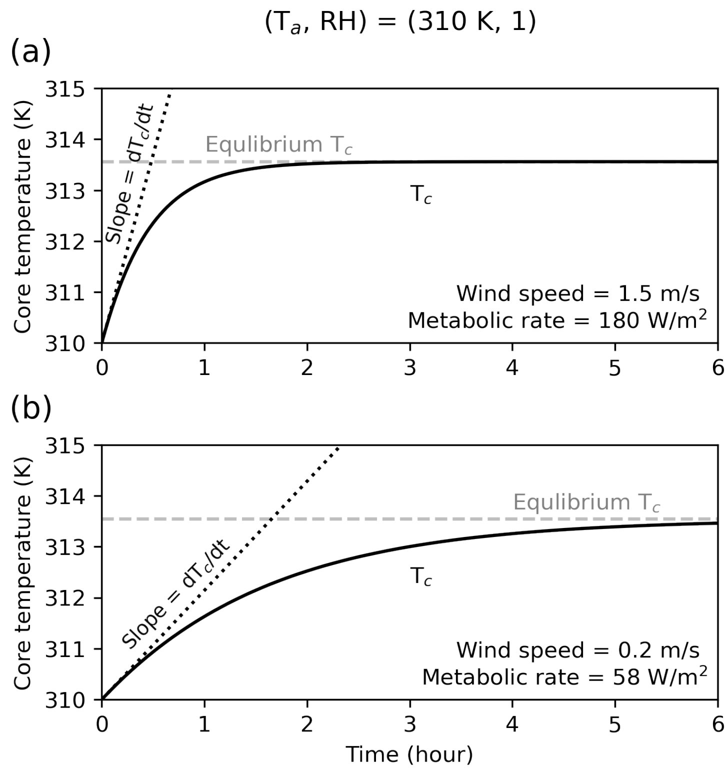

FIG. 2: (a) The black curve shows the time evolution of T_c for $(T_a, \mathrm{RH}) = (310\ \mathrm{K}, 1)$. The horizontal grey dashed line is the equilibrium T_c, and the dotted line is the tangent to the T_c curve at $t = 0$. These curves are generated using the default physiological parameters of the heat index, i.e., a metabolic rate of 180 W m^{-2} and a wind speed of 1.5 m s^{-1}. (b) Same as (a), but with a metabolic rate of 58 W m^{-2} and a wind speed of 0.2 m s^{-1}, which are typical of a person seated in a climate chamber.

core temperature (around 313.5 K) but a smaller initial warming rate (about 0.036 °C per minute, or 2.1 °C per hour). Under those conditions, it takes more than 6 hours to reach that equilibrium, as shown in Figure 2b.

We see, therefore, that it is inappropriate to linearly extrapolate an initially rising time series of core temperature. In practice, experiments on human subjects are stopped either after a few tens of minutes of hyperthermia (e.g., Cottle et al. 2022) or once the core temperature had risen by 2 °C (e.g., Meade et al. 2025). As Figures 2a and 2b demonstrate, this is not a sufficient time interval or temperature range to observe the possible equilibration of the core temperature in a laboratory setting. Indeed, if the data in either Figure 2a or 2b had been plotted up to only 2 °C of hyperthermia or a few tens of minutes (as in Meade et al. 2025; Cottle et al. 2022), the T_c curves could give the false impression of unbounded rise.

Since the term "uncompensable" has been routinely applied to a simple inflection followed by a rise in core temperature, a usage that diverges from its original intent of a lethal trajectory, we eschew that term. Instead, we describe environmental conditions as normothermic, hyperthermic, and lethal depending on whether the steady-state core temperature satisfies $T_c = 310$ K, 310 K $< T_c <$ 315 K, or $T_c \geq 315$ K, respectively. As shown by LR22, at a fixed metabolic rate and wind speed, there is a one-to-one mapping between the steady-state T_c and the instantaneous dT_c/dt at $T_c = 310$ K. Therefore, we can also define environmental conditions as normothermic, hyperthermic, and lethal depending on whether dT_c/dt at $T_c = 310$ K is $dT_c/dt = 0$, $0 < dT_c/dt < 0.178$ K min^{-1}, or $dT_c/dt \geq 0.178$ K min^{-1}, respectively, given the metabolic rate of 180 W m^{-2} and a wind speed of 1.5 m s^{-1} assumed by the heat index. The boundaries between these three regimes in T_a-RH space are indicated by black curves in Figure 1c.

b. Meaning of the heat index

So far, we have focused on the physiological model underlying the heat index. In the simplified version presented here, the physiological model is a function of air temperature and humidity that returns physiological state, which is either 1. the thermal resistance of the shell R_s that maintains normothermia as calculated from equations (3–5) or 2. the tendency of the core temperature dT_c/dt at $T_c = 310$ K as calculated from equation (6). The heat index itself is simply a convention for ranking those states.

In Figure 3a, we plot the isopleths of R_s (blue contours; normothermic) and dT_c/dt (red contours; hyperthermic and lethal) in T_a-RH space. The isopleths of R_s are expressed in units of m^2 K W^{-1} and dT_c/dt is expressed in units of K min^{-1}. The isopleths have been plotted at irregular intervals to coincide with significant physiological interpretations, to be discussed below. As expected, an increase in the air temperature or humidity leads to a decrease in R_s or an increase in dT_c/dt. Notably, the isopleth of $R_s = 0$ coincides with the isopleth of $dT_c/dt = 0$, which serves as the boundary between normothermic and hyperthermic.

With the isopleths in Figure 3a, we can explain how the heat index assigns a number to each state. Formally, the heat index is the air temperature, at a reference water vapor pressure of 1.6 kPa or saturation (whichever is lower), that induces the same physiological state (R_s and dT_c/dt) as the prevailing air temperature and humidity. To help find the same physiological state at the reference vapor pressure, we have added to Figure 3b a black curve marking the reference relative humidity of $\min(1.6\ \text{kPa}/p^*(T_a), 1)$.

We can now use Figure 3b to walk through some examples. Suppose we want to calculate the heat index for point A in the normothermic subspace. Point A lies on the isopleth $R_s = 0.0387$ m^2 K W^{-1}, and that isopleth intersects the black curve at point A'. Therefore, the temperature coordinate of A' is the heat index. As a second example, we can find the heat index for point B. Point B lies on the isopleth $dT_c/dt = 0.178$ K min^{-1}. Following this isopleth, we find its intersection with the 1.6 kPa contour at B'. The heat index is the temperature coordinate of B'. As a final example, consider point C. From C, we follow the isopleth of R_s, which intersects the black contour at C', located at RH = 1 because, at this temperature, the saturation vapor pressure p^* is less than 1.6 kPa. The heat index is the temperature coordinate of C'.

Note that the heat index can take on some very large values. This is a consequence of S79's choice of a constant reference vapor pressure of 1.6 kPa: at high air temperatures, the locus of points corresponding to 1.6 kPa (the black curve in Figure 3b) asymptotes to zero relative humidity, which is where the isopleths of dT_c/dt also flatten out. As a consequence, the heat index of point B, which is the temperature of point B', is more than 40 K higher than the air temperature at B. The value of 1.6 kPa was chosen by S79 to represent a typical vapor pressure in spaces designed for human comfort, but a different choice could have been made. For example, defining the reference relative humidity to be 50% would lead to the same ordering of physiological states, but very different numerical values of the heat index. In that case, the black curve would be a horizontal line at RH = 0.5 and the "heat index" for point B would equal the air temperature at point B.

In summary, the values of the heat index are just a convention for ordering and labeling physiological states. What really matters for human health, however, are the physiological states themselves, as predicted by the heat index's physiological model. We will discuss the interpretation of those states next.

c. Physiological outcomes

To aid in the interpretation of the physiological states, we can convert R_s and dT_c/dt to more familiar quantities. When R_s takes values between 0 and 0.0387 m^2 K W^{-1} (i.e., the old regions IV and V), R_s can be mapped to a skin blood flow b using equation (20) of LR22. Thus, in Figure 3c, we relabel the R_s isopleths of 0.0387, 0.0277, and 0 m^2 K W^{-1} as isopleths of blood flow with values of b_0, $1.5b_0$, and ∞, respectively, where $b_0 \equiv 0.57$ L min^{-1}. In S79, the isopleth $b = b_0$ is the boundary separating the clothed and naked states of the human (the boundary between regions III and IV), a point where the human model starts to ramp up its skin blood flow as a consequence of heat stress. Indeed, in the physiology literature (e.g., Johnson et al. 2014), the skin blood flow for a "resting and normothermic" human is estimated to be in the range of 0.25 to 0.5 L min^{-1}, so $b_0 \equiv 0.57$ L min^{-1} sits just above this range.

When $dT_c/dt > 0$ (at a core temperature of 310 K), there is a one-to-one map between dT_c/dt and the equilibrium core temperature (LR22). In other words, once dT_c/dt at $T_c = 310$ K is known, the equilibrium core temperature can be calculated, and vice versa, without any knowledge of (T_a,RH). In Figure 3c, the dT_c/dt isopleths of 0 and 0.178 K min^{-1} have been replaced by equilibrium core temperatures of 310 and 315 K, respectively.

Mathematically, we could replace all the dT_c/dt isopleths with the corresponding isopleths of steady-state core temperature, but this would make little sense physiologically since most of those temperatures would be unattainable by a living human. Since 315 K is often identified as the fatal core temperature (Ferris et al. 1938; Bouchama and Knochel

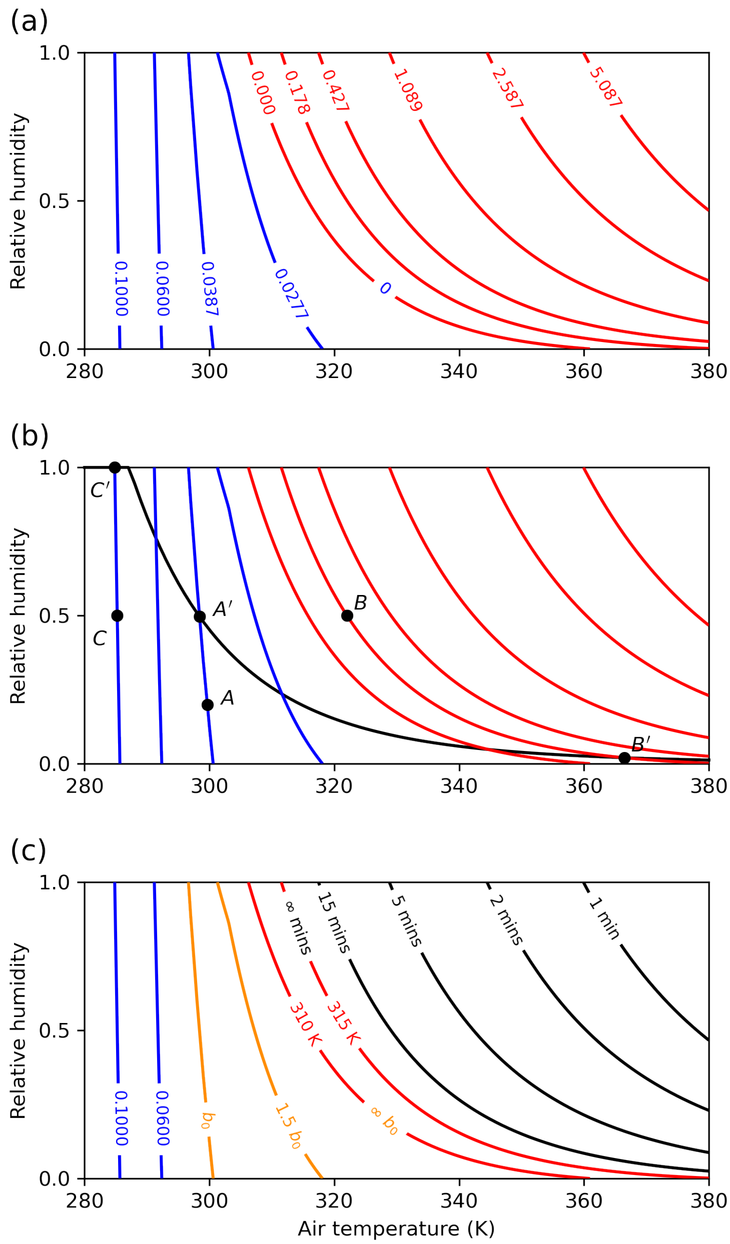

FIG. 3: (a) Isopleths of (blue) R_s in units of m^2 K W^{-1} and (red) dT_c/dt in units of K min^{-1} on axes of air temperature and humidity. (b) Same as the top panel, but with the addition of the (black) reference water vapor pressure. See the text for an explanation of the labeled points. (c) Isopleths of (blue) R_s, (orange) skin blood flow, (red) equilibrium T_c, and (black) the time for the core to reach a lethal temperature of 315 K. The normal skin blood flow, b_0, is defined here as 0.57 L min^{-1}.

2002), we are more interested in how fast the core temperature would hit this threshold. As shown in LR22, once dT_c/dt at $T_c = 310$ K is given, the time τ required for the core temperature to exceed 315 K is also uniquely determined. In Figure 3c, the dT_c/dt isopleths of 0.178, 0.427, 1.089, 2.587, and 5.087 K min^{-1} are replaced by $\tau = \infty$, 15, 5, 2, and 1 minute, respectively. Note that the $dT_c/dt = 0.178$ K min^{-1} isopleth corresponds to an equilibrium core temperature of 315 K, meaning the core temperature will never exceed 315 K, resulting in $\tau = \infty$ along this isopleth.

Again, the physiological outcomes we have derived here are based on the assumption of a healthy human walking in shade, in the presence of wind, and exhibiting idealized behaviors. In particular, this assumes a metabolic rate of 180 W m^{-2}, no solar insolation, a wind speed of 1.5 m s^{-1}, and the removal of clothing as needed to maximize cooling. Under these assumptions, if the idealized individual experiences some level of heat stress, any real person would experience that level of stress or higher.

6. Faster

LR22 released code to calculate the heat index in Fortran, R, and Python. In addition to suffering from the complexity, double values, and supersaturation described in section 2, the algorithm used in that code was also less efficient than it could have been. Here, we describe how a refactored algorithm can accelerate the computation of the heat index.

Section 4 described how to calculate the physiological state from the environmental air temperature T_a and relative humidity RH, and section 5b described how to calculate the heat index from the physiological state. In the pseudocode below, we will denote these two functions as PHYSIOLOGY and HEATINDEX, respectively. For brevity of notation, let us eliminate T_s and p_s from equations (3,4,5) to obtain

$$f_{\text{normo}}\left(T_a, \text{RH}, R_s\right) = 0. \tag{7}$$

Given any two of the three variables T_a, RH and R_s, this equation can be solved for the remaining unknown. Similarly, dividing equation 6 by C_c, we obtain

$$\frac{dT_c}{dt} = f_{\text{nonnormo}}\left(T_a, \text{RH}\right). \tag{8}$$

Given any two of the three variables dT_c/dt, T_a, and RH, this equation can be solved for the remaining unknown.

In the PHYSIOLOGY function, the first step is to calculate $f_{\text{nonnormo}}(T_a, \text{RH})$. If $f_{\text{nonnormo}}\left(T_a, \text{RH}\right) < 0$, the environmental condition is normothermic; otherwise, it is nonnormothermic (i.e., either hyperthermic or lethal). In normothermic conditions, dT_c/dt is set to zero, and equation (7) is solved for R_s. Otherwise, R_s is set to zero, and dT_c/dt retains its value. This procedure for calculating the physiological state is implemented as shown in Algorithm 1.

Algorithm 1 Physiological State

function PHYSIOLOGY(T_a, RH)
    $dT_c/dt \leftarrow f_{\text{nonnormo}}\left(T_a, \text{RH}\right)$

    if $dT_c/dt < 0$ **then** ▷ Normothermic case
        $dT_c/dt \leftarrow 0$
        $R_s \leftarrow$ solve for R_s: $f_{\text{normo}}\left(T_a, \text{RH}, R_s\right) = 0$
    else ▷ Nonnormothermic case
        $R_s \leftarrow 0$
    end if

    return $[R_s, dT_c/dt]$
end function

Next, we construct the HEATINDEX function. There are two possible implementations: one is short but computationally slow, while the other is longer but more efficient. In the short version, the algorithm contains a single line, as shown in Algorithm 2. In this approach, the details of the human physiology remain encapsulated within the PHYSIOLOGY function, making the HEATINDEX function independent of the specific physiological model. Even if the PHYSIOLOGY function were to change substantially, the HEATINDEX function would remain unchanged. On the other hand, there is a downside to this implementation, which is that it requires a nested root solver. The outer solver finds HI and the inner solver finds R_s and dT_c/dt. This nesting significantly increases execution time. This was the approach used in the code released by LR22.

The second approach is to embed the physiological model into the HEATINDEX function explicitly. Specifically, the function first calls PHYSIOLOGY to obtain R_s and dT_c/dt, and then solves for HI using equation (7) or (8) with the vapor pressure set at the reference level. This implementation avoids using nested root solvers, and so greatly reduces the computational expense. The implementation is presented in Algorithm 3.

Algorithm 2 Heat Index (short, but slow)

function HEATINDEX(T_a, RH)
  return solve for HI: PHYSIOLOGY $(\mathrm{HI}, \min(1.6\ \mathrm{kPa}/p^*(\mathrm{HI}), 1)) =$ PHYSIOLOGY (T_a, RH)
end function

Algorithm 3 Heat Index (long, but fast)

function HEATINDEX(T_a, RH)
  $[R_s, dT_c/dt] \leftarrow$ PHYSIOLOGY (T_a, RH)

  if $dT_c/dt = 0$ **then** ▷ Normothermic case
    HI $\leftarrow$ solve for HI: $f_{\mathrm{normo}}(\mathrm{HI}, \min(1.6\ \mathrm{kPa}/p^*(\mathrm{HI}), 1), R_s) = 0$
  else ▷ Nonnormothermic case
    HI $\leftarrow$ solve for HI: $dT_c/dt = f_{\mathrm{nonnormo}}(\mathrm{HI}, \min(1.6\ \mathrm{kPa}/p^*(\mathrm{HI}), 1))$
  end if

  return HI
end function

In addition to employing this refactored algorithm, we use Brent's method as the root solver, which typically converges to solutions significantly faster than the traditional bisection method (Brent 1971). In comparison to the Fortran, Python and R code released by LR22, this new approach is faster by factors of ~100, ~1,000 and ~10,000, respectively. Recently, Lanzante (2024) proposed using multiple polynomial approximations or a lookup table for calculating LR22's extended heat index, demonstrating speed improvements over LR22's Fortran code by factors of ~800 (polynomials) and ~2,000 (lookup table). Practically, polynomial approximations or lookup tables offer sufficient accuracy and efficiency for general heat index calculations. However, similar to the limitations in Rothfusz (1990)'s polynomial, the work presented by Lanzante (2024) is valid for air temperatures only below 331 K. Furthermore, our algorithm-based code provides the flexibility to adjust to other scenarios, such as the different metabolic rates and windspeeds considered in Lu and Romps (2023a).

7. Discussion

Since the heat index was introduced by S79, there have been a couple efforts to remedy its deficiencies. The first was Rothfusz (1990), which introduced a computationally efficient polynomial fit to the heat index values presented in Table 2 of S79. This led, however, to the use of that polynomial to calculate extrapolated and, in hindsight, erroneous values of the heat index. This was fixed by LR22, which extended the calculation of the heat index to all combinations of temperature and humidity.

In so doing, however, LR22 inadvertently retained the double-valued problem in the original algorithm of S79 (see Figure 1a), and LR22 also introduced new unphysical phenomena in the solutions: the supersaturation of skin and clothing at cold temperatures (see Figure 1a). Furthermore, in attempting to hew as closely as possible to the model of S79, LR22 retained the considerable complexity of the original model, and the algorithm used in the code of LR22 was computationally inefficient.

Here, we have corrected those deficiencies. The complexity of S79's model, created by the inclusion of clothing as a distinct layer, has been eliminated. The simplified model presented here replaces the two layers of skin and clothing with a single shell. This leads to tolerable changes to the values of the heat index, as shown in Figure 1b. Furthermore, this simplification leaves the values of the heat index completely unaltered for all air temperatures above 300 K (27 °C or 81 °F). In addition, refactoring the algorithm has substantially increased its computational speed, which makes it far more efficient than the original implementation and, unlike polynomial approximations, preserves the full flexibility of the underlying model implemented in open-source code.

The heat index model represents one end of a spectrum of physiology models: it was intentionally designed to represent a young, healthy adult with idealized physiology and behavior, but this is just one possible modeling choice. For behavior, the heat index model assumes that an individual remains clothed in mild conditions (in regions I, II and III) but removes clothing in hot conditions (in regions IV, V and VI). Other models treat clothing differently: Ravanelli et al. (2019); Guzman-Echavarria et al. (2024) always include clothing; Vanos et al. (2023) include clothing when evaluating livability but assume a naked subject when assessing survivability; and Fan and McColl (2024) assume a naked subject in all cases. For physiology, the sweating rate in the heat index model can reach as high as 3.2 L hr^{-1} in a normothermic state and 4.3 L hr^{-1} in a hyperthermic state (see Appendix B for a discussion), which is largely consistent with the maximum observed sweating rates of 2–4 L hr^{-1} for young adults (Mack and Nadel 1994; Baker et al. 2016). Other studies have imposed upper limits on the sweating rate representing average population values—for example, 1.4 L hr^{-1} in Fan and McColl (2024) and 0.75 L hr^{-1} in Vanos et al. (2023). These choices make those models more representative of the average population, but they will overestimate heat stress in healthier individuals and underestimate it in less healthy individuals. In contrast, the heat index model represents young, healthy adults with the objective of representing the upper bound of human thermoregulatory capacity.

Acknowledgments. We thank the editor, J. W. Nielsen-Gammon, and three anonymous reviewers for their feedback on the paper.

Data availability statement. The source code for computing the heat index is publicly available on GitHub at https://github.com/davidromps/heatindex. The software is also distributed as packages for R and Python, available from CRAN (https://cran.r-project.org/web/packages/heatindex) and PyPI (https://pypi.org/project/heatindex), respectively. Documentation and usage examples can be found at the package homepage: https://heatindex.org/.

APPENDIX A

Double-valued problem

S79 defined the heat index in the regions III and IV shown in Figure 1a. In region III, the human model is clothed and modulates its clothing resistance R_f to maintain thermal equilibrium. In region IV, the model assumes a naked human who adjusts skin resistance R_s to achieve thermal equilibrium.

Figure A1a gives a schematic rendering (not-to-scale) of the R_f (orange) and R_s (blue) values in the heat index model of S79. The R_f surface has a higher value in the low temperature regime, indicating that a person needs thicker clothing to maintain a standard core temperature. As the air temperature rises, the R_f surface declines and eventually hits zero, beyond which there are decreases in R_s. According to S79, the end of region III is defined as the (T_a, RH) locus such that $R_f = 0$, and the beginning of region IV is defined as the (T_a, RH) locus such that R_s starts to decline from 0.0387 $\mathrm{m}^2\mathrm{K}\ \mathrm{W}^{-1}$. As can be seen in Figure A1a, these two boundaries are not the same. Indeed, there is an area between those two boundaries (colored green) that qualifies as both region III and region IV, leading to the double-valued behavior. As a reminder, this schematic diagram is not to scale; the green area is plotted to scale in Figure A1b using “skew-T RH” coordinates. The width of the green area ranges from 0.02 K (at RH = 0) to 0.04 K (at RH = 1).

When (T_a, RH) falls within the green area, the model has two ways to achieve thermal equilibrium: one is to wear clothes ($R_f > 0$) while maintaining the lowest skin blood flow (maximum R_s), and the other is to shed all clothing ($R_f = 0$) and increase the skin blood flow (reduce R_s). This is a pathological result: the model claims that wearing clothes (warming effect) is somehow equivalent to being naked with a higher skin blood flow (both cooling effects). The reason for this bad behavior is that S79's model assigns the boundary layer of air above exposed skin a much higher heat transfer coefficient (17.4 W K^{-1} m^{-2}) when the body is partially clothed than when it is naked (12.3 W K^{-1} m^{-2}).

A direct consequence of this is that the heat index becomes double-valued in the green area, meaning a given (T_a, RH) can be mapped to two possible heat index values. This occurs because the isopleths of R_f and R_s in this region are not parallel. When a specific (T_a, RH) pair is given, the heat index can be determined either by tracing the R_f isopleth or the R_s isopleth, leading to different results. Figure A2a gives another schematic rendering of the double-valued region (green), along with the curve of constant vapor pressure of 1.6 kPa (red). For an arbitrary point A in the green region, we can trace the R_f isopleth (orange) to find its heat index at B_1, or we can trace the R_s isopleth (blue) to find its second heat index at B_2. In practice, the difference between the two possible heat index values is less than 0.03 K (the horizontal width of the red curve inside the green area). On the other hand, this double-valued behavior prevents the heat index from being a function and leads to problems with numerical implementations.

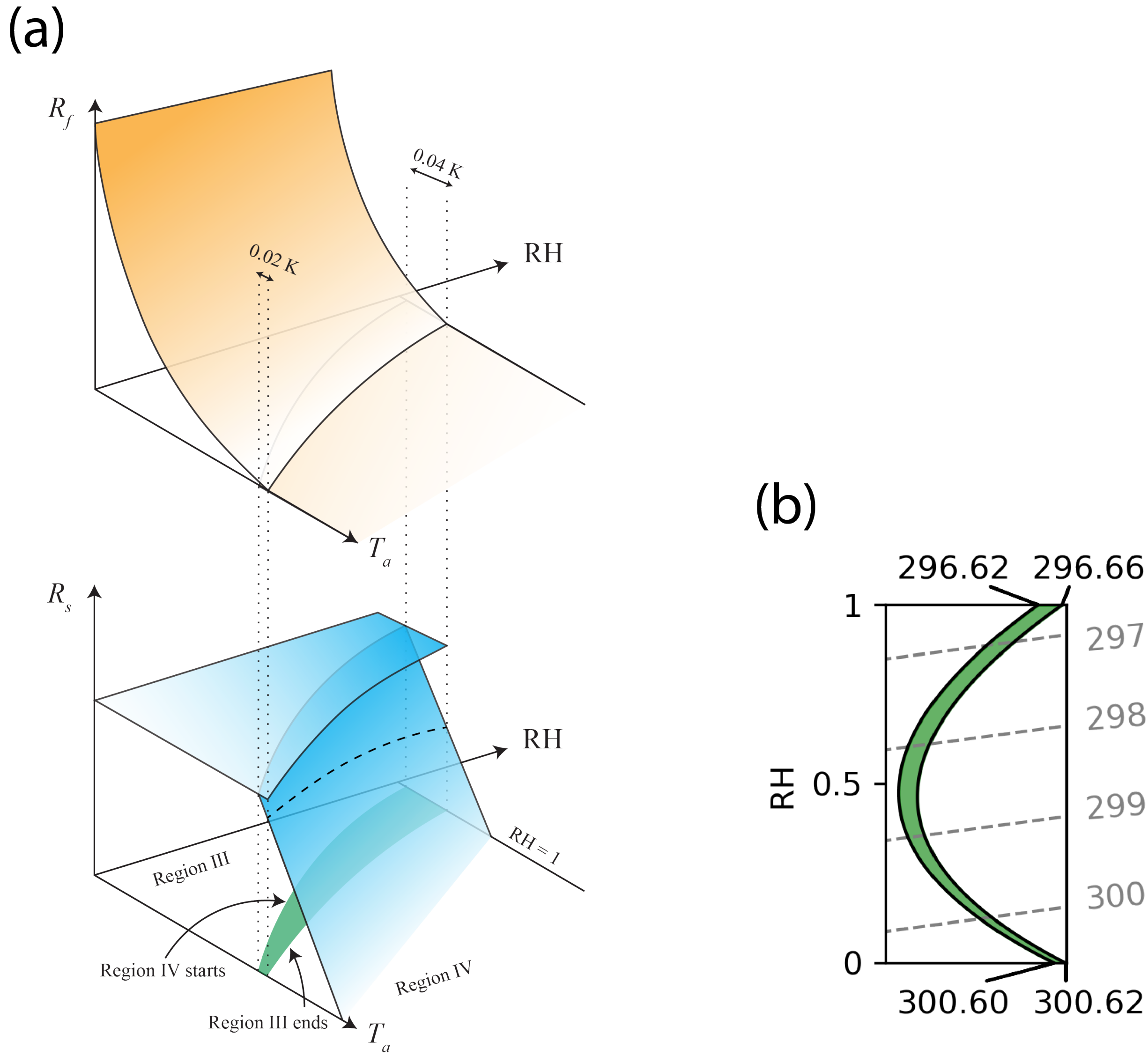

Fig. A1: (a) A hand-drawn schematic diagram showing the R_f (orange) and R_s (blue) surfaces near the interface of regions III and IV. The green area shows where the two surfaces overlap with themselves, which is also where the heat index is double-valued. The width of the green region ranges from 0.02 K (at RH = 0) to 0.04 K (at RH = 1). (b) A "skew-T RH" diagram showing where the heat index is double-valued. The dashed grey lines are air-temperature isopleths ranging from 297 to 300 K, as labeled by the grey numbers. The numbers along the top and bottom of the diagram are the air temperatures of the end points of the two curves bounding the double-valued area.

At the implementation level, the R, Python, and Fortran codes released with LR22 all resolve the double-valued problem by following R_f isopleths to locate the heat index inside the green area. For example, for point A, the codes follow the R_f isopleth to B_1, effectively choosing the clothing strategy in the green area. However, this implementation creates an additional grey area immediately to the right of the green (Figure A2b), within which the codes give an inconsistent prediction or even the wrong heat index. To demonstrate, consider point C_2 in the grey area. It lies in region IV (unclothed), so the correct procedure would be to trace the R_s isopleth (blue) and find its heat index at D_2. This indeed is what LR22's R implementation does: for the point C_2, the code returns the temperature of the same point D_2 as the heat index, and reports that the human is in region IV (unclothed). However, using the same implementation, if we input D_2, the code returns the temperature at D_2 as the heat index, but reports that the human is in region III (clothed) — this is because the code chooses clothing when the input is in green. So, under this implementation, the same heat index will be given different interpretations as to whether the human is naked or clothed. The Python and Fortran implementations are even worse: the codes perform a bisection search along the red curve trying to bracket the heat index for C_2; if the trial is left of D_1, they infer clothed conditions and shift right, whereas if it is right of D_1, they detect a lower R_s and shift left. This procedure invariably converges on D_1, which shares neither the same R_s nor the same R_f as C_2 and thus violates equation 1.

To illustrate another impact, consider finding the heat index for points C_1 and C_2 in the grey area and C_3 just inside the green area. The R code maps them to D_1, D_2, and D_1, respectively. Even though C_2 is hotter than C_3, the R code assigns a heat index for C_2 that is lower than that for C_3. So, this implementation reverses the heat ranking for some points within the grey and green area. The Python and Fortran implementations also have bad behaviors: all the three heat indices collapse to D_1. Indeed, those codes report a heat index corresponding to the temperature of D_1 for all points in the grey area, implying an identical heat ranking for an entire two-dimensional subset of T_a-RH space.

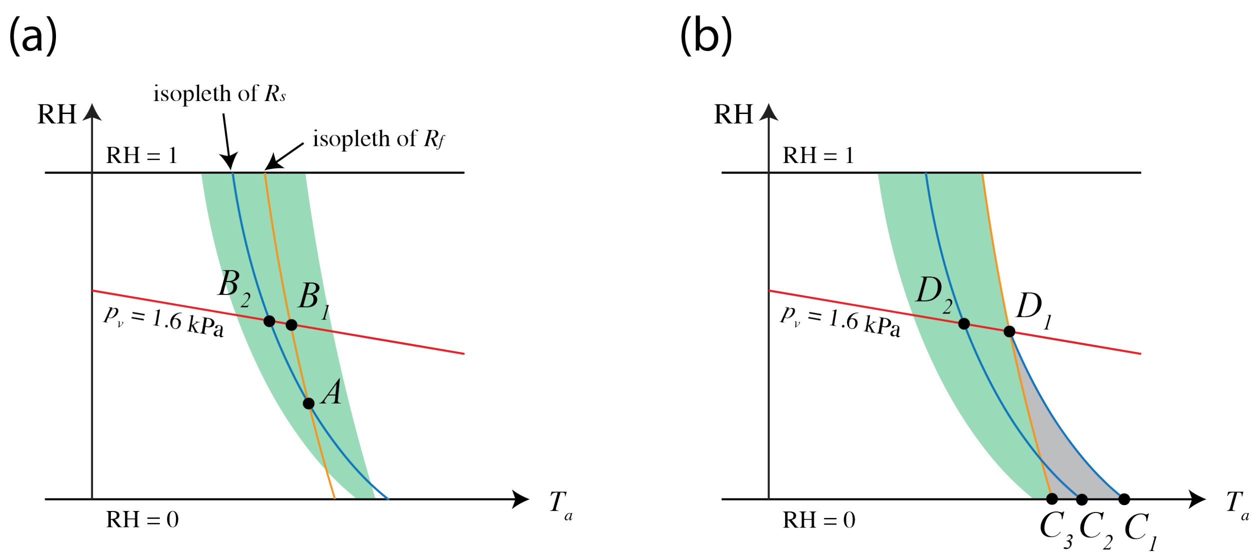

FIG. A2: (a) A hand-drawn schematic diagram showing the region where the heat index is double-valued (green) and the curve of constant vapor pressure p_v = 1.6 kPa (red). For an arbitrary point A in the green region, we can trace the R_f isopleth (orange) to find its heat index at B_1, or we can trace the R_s isopleth (blue) to find its second heat index at B_2. (b) The green area and the red curve are the same as in (a). The extra grey area is bounded by RH = 0 (C_1C_3, black), an R_f isopleth (C_3D_1, orange) and an R_s isopleth (D_1C_1, blue). The three points C_1, C_2 and C_3 are on the RH = 0 axis, and the two points D_1 and D_2 are on the p_v = 1.6 kPa curve. See the main text for their interpretations.

The reason that the R_f and R_s surfaces overlap is that S79 gave regions III and IV different values for several parameters. For each of those parameters, Table A1 lists their names (first column), their values in regions III (second column), and their values in region IV (third column). The interpretation of the parameters is provided in the caption, and the details can be found in LR22. For the purpose of this paper, we will simply focus on their values across the interface. For example, the heat transfer coefficient h_c has a value of 17.4 (in SI units) in region III, while it has a different value of 12.3 in region IV. Similarly, Z_s has a value of 52.1 in region III, while in region IV it follows an empirical relation $\left(6\times10^8\right)R_s^5$, which does not equal 52.1 when R_s takes its value of 0.0387 for region III. These parameters were chosen by S79, and when LR22 extended the definition of heat index to cover regions I, II, V, and VI, these parameters were retained to ensure backward compatibility.

One possible fix to this double-valued problem would be to render the parameters in Table A1 continuous, but that would have still left the problem of supersaturated clothing. In this article, we take the alternative approach of extending the domain of equations (3-5) to cover colder temperatures. Graphically, this is equivalent to extending the sloping blue R_s surface to lower temperatures and eliminating the R_f surface in Figure A1a. This guarantees that the physiological model is continuous and single-valued, which ensures that the heat index is continuous and single-valued as well.

Variable	Value in region III	Value in region IV
Z_s	52.1 $\mathrm{m^2 Pa\,W^{-1}}$	$(6\times10^8\ \mathrm{Pa\,W^4 m^{-8} K^{-5}})R_s^5$
ϕ_{rad}	0.85	0.8
$\overline{\phi}_{\mathrm{rad}}$	0.79	N/A
h_c	17.4 $\mathrm{W\,K^{-1}m^{-2}}$	12.3 $\mathrm{W\,K^{-1}m^{-2}}$
$\overline{h}_c$	11.6 $\mathrm{W\,K^{-1}m^{-2}}$	N/A
ϕ	0.84	N/A

Table A1: Physiological parameters in regions III and IV as presented in S79 and LR22. Interpretation of each symbol: Z_s is the resistance to mass transfer through the skin, ϕ_{rad} ($\overline{\phi}_{\mathrm{rad}}$) is the effective fraction of exposed skin (clothing) exchanging longwave radiation with the surroundings, h_c ($\overline{h}_c$) is the heat transfer coefficient between surface of exposed skin (clothing) and air, and ϕ is fraction of skin covered by clothing. The variables $\overline{\phi}_{\mathrm{rad}}$, $\overline{h}_c$ and ϕ do not have values in region IV because the model is in a naked state.

APPENDIX B

Finite sweating rate and skin blood flow

a. Finite sweating rate

The heat index model does not explicitly set a limit on the sweating rate, but it has a maximum value. To understand why, recall that the heat index is defined as the air temperature at a water vapor pressure of 1.6 kPa that would produce the same response. Here, the "response" is measured at a core temperature of 310 K, even for conditions that would induce hyperthermia. Two hyperthermic conditions are equivalent if they produce the same positive dT_c/dt at an initial temperature of T_c = 310 K. In such hyperthermic conditions, the skin temperature is fully wetted at a temperature of 310 K. In a given wind — such as 1.5 m $\mathrm{s^{-1}}$ assumed by the heat index — a fully wetted surface at a fixed temperature has a maximum evaporation rate, which is obtained when the air has zero humidity. Furthermore, that evaporation rate is independent of the air temperature. For the heat index model, that maximum evaporation rate for wetted skin at 310 K is 3.2 L $\mathrm{hr^{-1}}$. Thus, this is the maximum sweating rate implied by the heat index model at a normal core temperature. This is only marginally higher than the maximum sweating rate implied by the original formulation by Steadman (1979), which was a rate of 2.8 L $\mathrm{hr^{-1}}$ occurring at the hot-dry end of region IV.

If we wish to calculate the equilibrium core temperature for the heat index model in hyperthermic conditions, or the time to death (defined as the time it takes the core temperature to rise to 315 K; see section 5c), then we must perform calculations with the heat index model in which the fully wetted skin is as warm as 315 K. In the heat index model, the maximum evaporation rate for wetted skin at 315 K is 4.3 L $\mathrm{hr^{-1}}$. Therefore, this is the maximum sweating rate implied by the heat index model during a state of hyperthermia.

Sweating rates as high as 3.2 and 4.3 L $\mathrm{hr^{-1}}$ are at the high end of, but largely consistent with, observed maximum sweating rates for healthy adults. Maximum sweating rates in healthy adults are typically measured to be in the range of 2–4 L $\mathrm{hr^{-1}}$ (Mack and Nadel 1994; Baker et al. 2016), with rare short-term values approaching 6 L $\mathrm{hr^{-1}}$ during strenuous exercise (Baker et al. 2016).

Not all individuals, however, have this level of sweating capacity. To account for such variability, several physiological models impose fixed upper limits on sweating using average values. For example, Fan and McColl (2024) assumes a maximum of 1.4 L $\mathrm{h^{-1}}$, while Vanos et al. (2023) uses 0.75 L $\mathrm{h^{-1}}$. These choices make the models more representative of the average population, but they also cause them to overestimate heat stress in fitter individuals and underestimate it in those with health limitations. By contrast, the heat index model was intentionally designed to represent young, healthy adults. This design choice inevitably underestimates heat stress for less fit individuals, yet both approaches are valid modeling choices; we do not argue that either is intrinsically more "correct" than the other.

Nevertheless, it is helpful to show what sweating rates are reached in the temperature-humidity space, and what the implications are once the sweating rate is capped. In Figure B1, we therefore show isopleths of the evaporation rate assumed by the heat index, followed by results when it is capped at moderate values of 1 L $\mathrm{hr^{-1}}$. Figure B1a shows the evaporation rate assumed by the heat index (solid blue curves). The dashed blue curves correspond to negative values—conditions under which water vapor from the air condenses onto the skin and releases latent heat. In such cases, the model requires no sweat production from the human.

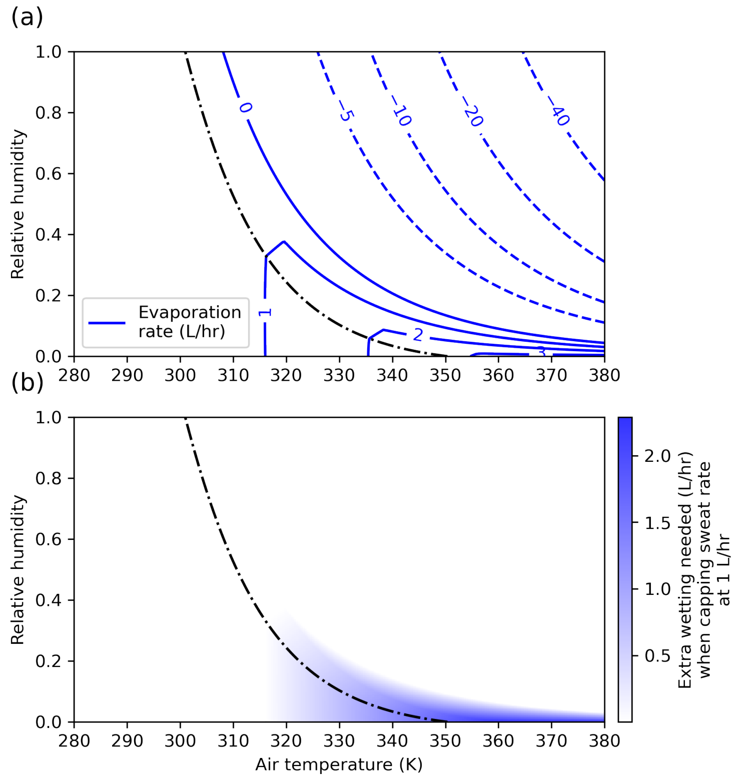

FIG. B1: (a) Evaporation rate (L hr^{-1}) assumed by the heat index. Negative values—shown with dashed curves—indicate condensation of atmospheric water vapor onto the skin. The black dotted curve marks the boundary where Steadman's original model begins to break down. (b) Same black dotted curve, overlaid with a heat map showing the additional wetting required when the sweating rate is capped at 1 L hr^{-1}.

From the figure, a sweating rate of 1 L hr^{-1} is reached when air temperature exceeds 316 K (43 °C, 109 °F) and relative humidity drops below 38%. A rate of 2 L hr^{-1} occurs above 335 K (62 °C, 143 °F) when relative humidity is below 9%. Finally, a rate of 3 L hr^{-1} occurs above 355 K (82 °C, 179 °F) when relative humidity is below 1%.

If an individual can only sustain sweating at 1 L hr^{-1}, they would need to supplement evaporative cooling manually (e.g., by misting themselves) to satisfy the heat index's assumption of wetted skin. Figure B1b shows the resulting "extra wetting rate" needed to satisfy the model assumptions under this constraint. The required supplemental wetting ranges from 0 to 2.2 L hr^{-1} in the hot and dry conditions. If such misting is not available, readers should recognize that the heat index predictions become unreliable once this physiological limit is exceeded.

In the analysis above, we have assumed a sweating efficiency (the fraction of sweat that is evaporated) of 100%. Laboratory studies in physiology have measured sweating efficiency (η) as a function of skin wettedness (ω) under controlled conditions and most have found that efficiency tends to decline as wettedness increases (Candas et al. 1979a,b; Soto 1982; Frye and Kamon 1983; Alber-Wallerström and Holmér 1985). The ISO 7933 standard adopts a simple empirical relation, $\eta = 1 - \omega^2/2$ for $\omega \leq 1$, which yields $\eta = 0.5$ at full skin wettedness and has been widely used in heat-stress assessment (e.g., Cramer and Jay 2019; Vanos et al. 2023). However, experimental measurements show substantial variability depending on environmental conditions, particularly airflow. Across five available laboratory studies (Candas et al. 1979a,b; Soto 1982; Frye and Kamon 1983; Alber-Wallerström and Holmér 1985) with wind speeds ranging from 0.2 to 1 m s^{-1}, sweating efficiency at $\omega = 1$ spans a broad range, from approximately $\eta = 0.5$ attained at 0.2 m s^{-1} to as high as $\eta = 0.95$ at 1 m s^{-1}. Because the heat index model represents a person walking in a wind speed of 1.5 m s^{-1}, which exceeds the airflow in these laboratory experiments, sweating efficiency in this context is expected to lie near the upper end of the observed range. Accordingly, for simplicity, we approximate the sweating efficiency as $\eta = 1$.

b. Finite skin blood flow

The heat index model assumes that skin blood flow can increase as needed—ranging from a baseline of approximately 0.57 L min^{-1} up to infinity—to regulate the core temperature. In reality, the highest skin blood flow measured in young, healthy adults is about 6–8 L min^{-1} (Detry et al. 1972; Rowell 1974; Taylor et al. 1984; Minson et al. 1998), as also reported by contemporary reviews (e.g., Johnson and Proppe 1994; Charkoudian 2003; Johnson et al. 2014; Petrofsky 2017; Chaseling et al. 2020; Low et al. 2020). Approximating this upper limit as infinite is a mathematical convenience. It is equivalent to treating the small thermal resistance of the skin ($R_s \approx 0.003$ m^{2}K W^{-1}) as zero resistance.

The practical insignificance of this approximation is demonstrated in Figure B2. Figure B2a shows the skin blood flow (orange curves) implied by the heat index, and Figure B2b shows the impact when a strict physiological cap of 6 L min^{-1} is imposed. Two main changes emerge under the cap. First, the boundaries separating normothermic, hyperthermic, and lethal conditions shift leftward (red curves vs. black curves). Second, the predicted equilibrium core temperature increases modestly, as shown by the orange heat map.

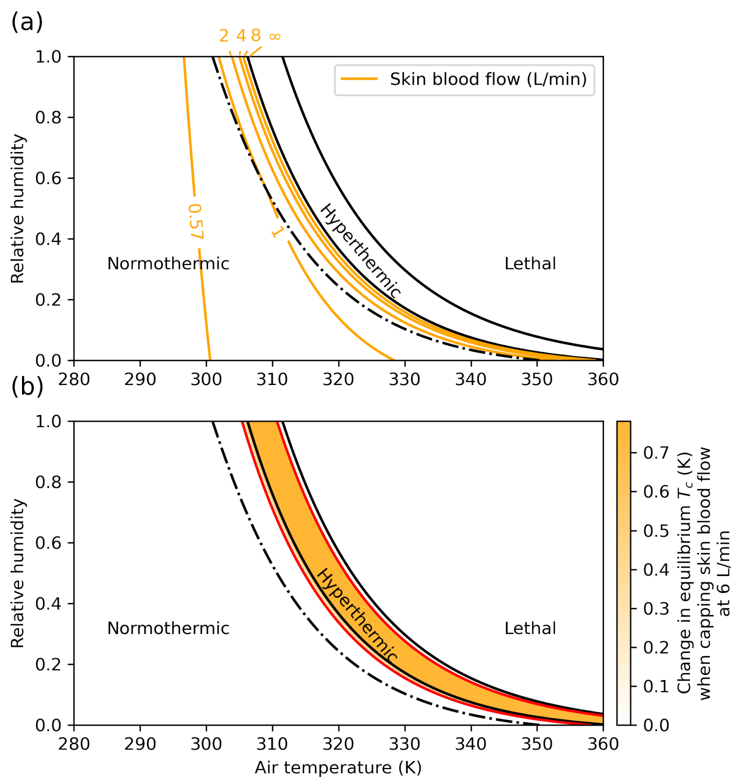

Fig. B2: (a) Orange curves show the skin blood flow assumed by the heat index. Solid black curves mark the boundaries separating normothermic, hyperthermic, and lethal conditions, and the dotted black curve indicates where Steadman's original formulation begins to break down. (b) The same black contours overlaid with a heat map for hyperthermic states showing the change in equilibrium core temperature when skin blood flow is capped at 6 L min^{-1}. In the lethal region where equilibrium T_c is undefined, the heat map is left blank. Red curves show the shifted boundaries of the three regions under this constraint.

As seen in Figure B2a, the isopleths for 4, 8, and ∞ L min^{-1} stack very close to one another compared with the spread of the 0.57, 1 and 2 L min^{-1} curves. Consequently, choosing a realistic threshold (e.g., 6 or 8 L min^{-1}) versus an infinite threshold makes little practical difference. Quantitatively, as shown in the right panel, imposing a 6 L min^{-1} limit shifts the boundaries separating normothermic, hyperthermic, and lethal conditions leftward by only ~1 K across most humidity levels. Furthermore, the predicted equilibrium core temperature in the hyperthermic region rises by only ~0.8 K compared to the unconstrained model. From low to high air temperatures, the difference grows from zero and quickly plateaus at about 0.8 K. In the lethal region where equilibrium T_c is undefined, the heat map is left blank.

In the above analysis, we present the effects of finite sweating rate and finite skin blood flow separately. We also examined their combined effect by imposing both constraints simultaneously. The resulting figure is visually indistinguishable from simply overlaying Figures B1b and B2b. In particular, the region requiring additional external wetting (blue shading in Figure B1b) is slightly reduced because hyperthermic and lethal conditions are reached at colder air temperatures. The value of the required wetting also changes slightly: it decreases by at most 0.15 L hr^{-1} for air temperature less than 360 K due to a decrease in the skin temperature, and only within regions that are hyperthermic or lethal. This demonstrates that the interaction between finite skin blood flow and sweating is weak, and that treating these constraints separately provides a clear yet accurate demonstration of their effects.

References

Alber-Wallerström, B., and I. Holmér, 1985: Efficiency of sweat evaporation in unacclimatized man working in a hot humid environment. *European Journal of Applied Physiology and Occupational Physiology*, **54 (5)**, 480–487.

Baker, L. B., K. A. Barnes, M. L. Anderson, D. H. Passe, and J. R. Stofan, 2016: Normative data for regional sweat sodium concentration and whole-body sweating rate in athletes. *Journal of Sports Sciences*, **34 (4)**, 358–368.

Bouchama, A., and J. P. Knochel, 2002: Heat stroke. *New England Journal of Medicine*, **346 (25)**, 1978–1988.

Brent, R. P., 1971: An algorithm with guaranteed convergence for finding a zero of a function. *The Computer Journal*, **14 (4)**, 422–425.

Candas, V., J. Libert, and J. Vogt, 1979a: Human skin wettedness and evaporative efficiency of sweating. *Journal of Applied Physiology*, **46 (3)**, 522–528.

Candas, V., J. Libert, and J. Vogt, 1979b: Influence of air velocity and heat acclimation on human skin wettedness and sweating efficiency. *Journal of Applied Physiology*, **47 (6)**, 1194–1200.

Charkoudian, N., 2003: Skin blood flow in adult human thermoregulation: how it works, when it does not, and why. *Mayo clinic proceedings*, Elsevier, Vol. 78, 603–612.

Chaseling, G. K., C. G. Crandall, and D. Gagnon, 2020: Skin blood flow measurements during heat stress: technical and analytical considerations. *American Journal of Physiology-regulatory, Integrative and Comparative Physiology*, **318 (1)**, R57–R69.

Cheung, S. S., T. M. McLellan, and S. Tenaglia, 2000: The thermophysiology of uncompensable heat stress: physiological manipulations and individual characteristics. *Sports Medicine*, **29**, 329–359.

Cottle, R. M., Z. S. Lichter, D. J. Vecellio, S. T. Wolf, and W. L. Kenney, 2022: Core temperature responses to compensable versus uncompensable heat stress in young adults (PSU HEAT Project). *Journal of Applied Physiology*, **133 (4)**, 1011–1018.

Cramer, M. N., D. Gagnon, O. Laitano, and C. G. Crandall, 2022: Human temperature regulation under heat stress in health, disease, and injury. *Physiological Reviews*.

Cramer, M. N., and O. Jay, 2019: Partitional calorimetry. *Journal of Applied Physiology*, **126 (2)**, 267–277.

Detry, J., G. L. Brengelmann, L. B. Rowell, and C. Wyss, 1972: Skin and muscle components of forearm blood flow in directly heated resting man. *Journal of Applied Physiology*, **32 (4)**, 506–511.

Fan, Y., and K. A. McColl, 2024: Widespread outdoor exposure to uncompensable heat stress with warming. *Communications Earth & Environment*, **5 (1)**, 762.

Ferris, E. B., M. A. Blankenhorn, H. W. Robinson, and G. E. Cullen, 1938: Heat stroke: clinical and chemical observations on 44 cases. *The Journal of Clinical Investigation*, **17 (3)**, 249–262.

Foster, J., S. G. Hodder, A. B. Lloyd, and G. Havenith, 2020: Individual responses to heat stress: implications for hyperthermia and physical work capacity. *Frontiers in Physiology*, **11**, 541 483.

Frye, A., and E. Kamon, 1983: Sweating efficiency in acclimated men and women exercising in humid and dry heat. *Journal of Applied Physiology*, **54 (4)**, 972–977.

Guzman-Echavarria, G., A. Middel, D. J. Vecellio, and J. Vanos, 2024: The development of an adaptive heat stress compensability classification applied to the united states. *International Journal of Biometeorology*, 1–15.

Johnson, J. M., C. T. Minson, and D. L. Kellogg Jr, 2014: Cutaneous vasodilator and vasoconstrictor mechanisms in temperature regulation. *Comprehensive Physiology*, **4 (1)**, 33–89.

Johnson, J. M., and D. W. Proppe, 1994: Cardiovascular adjustments to heat stress. *Comprehensive Physiology*, 215–243, https://doi.org/https://doi.org/10.1002/j.2040-4603.1994.tb01157.x.

Kraning, K. K., and R. R. Gonzalez, 1991: Physiological consequences of intermittent exercise during compensable and uncompensable heat stress. *Journal of Applied Physiology*, **71 (6)**, 2138–2145.

Lanzante, J. R., 2024: Efficient and accurate shortcuts for calculating the extended heat index. *Journal of Applied Meteorology and Climatology*, **63 (12)**, 1589–1594.

Low, D. A., H. Jones, N. T. Cable, L. M. Alexander, and W. L. Kenney, 2020: Historical reviews of the assessment of human cardiovascular function: interrogation and understanding of the control of skin blood flow. *European Journal of Applied Physiology*, **120 (1)**, 1–16.

Lu, Y.-C., and D. M. Romps, 2022: Extending the heat index. *Journal of Applied Meteorology and Climatology*, **61 (10)**, 1367–1383, https://doi.org/10.1175/jamc-d-22-0021.1.

Lu, Y.-C., and D. M. Romps, 2023a: Is a wet-bulb temperature of 35 °C the correct threshold for human survivability? *Environmental Research Letters*, **18 (9)**, 094 021, https://doi.org/10.1088/1748-9326/ace83c, URL https://doi.org/10.1088/1748-9326/ace83c.

Lu, Y.-C., and D. M. Romps, 2023b: Predicting fatal heat and humidity using the heat index model. *Journal of Applied Physiology*, **134 (3)**, 649–656, https://doi.org/10.1152/japplphysiol.00417.2022, URL https://doi.org/10.1152/japplphysiol.00417.2022.

Mack, G. W., and E. R. Nadel, 1994: Body fluid balance during heat stress in humans. *Comprehensive Physiology*, 187–214, https://doi.org/https://doi.org/10.1002/cphy.cp040110.

Meade, R. D., and Coauthors, 2025: Validating new limits for human thermoregulation. *Proceedings of the National Academy of Sciences*, **122 (14)**, e2421281 122.

Minson, C. T., S. L. Wladkowski, A. F. Cardell, J. A. Pawelczyk, and W. L. Kenney, 1998: Age alters the cardiovascular response to direct passive heating. *Journal of Applied Physiology*, **84 (4)**, 1323–1332.

Nunneley, S. A., 1970: Head cooling in work and heat stress. URL https://etd.ohiolink.edu/acprod/odb_etd/ws/send_file/send?accession=osu1729692384675986.

Parsons, K., 2014: *Human thermal environments: The effects of hot, moderate, and cold environments on human health, comfort, and performance*. CRC press.

Petrofsky, J. S., 2017: Control of skin blood flow. *Textbook of Aging Skin*, M. A. Farage, K. W. Miller, and H. I. Maibach, Eds., Springer, 1091–1104, https://doi.org/10.1007/978-3-662-47398-6.

Ravanelli, N., G. Coombs, P. Imbeault, and O. Jay, 2019: Thermoregulatory adaptations with progressive heat acclimation are predominantly evident in uncompensable, but not compensable, conditions. *Journal of Applied Physiology*, **127 (4)**, 1095–1106.

Ravanelli, N. M., D. Gagnon, S. G. Hodder, G. Havenith, and O. Jay, 2017: The biophysical and physiological basis for mitigated elevations in heart rate with electric fan use in extreme heat and humidity. *International Journal of Biometeorology*, **61 (2)**, 313–323.

Romps, D. M., and Y.-C. Lu, 2022: Chronically underestimated: a reassessment of US heat waves using the extended heat index. *Environmental Research Letters*, **17 (9)**, 094 017, https://doi.org/10.1088/1748-9326/ac8945, URL https://doi.org/10.1088/1748-9326/ac8945.

Rothfusz, L. P., 1990: The Heat Index "equation" (or, more than you ever wanted to know about Heat Index). Technical Attachment SR 90-23, NWS Southern Region Headquarters, Forth Worth, TX. URL https://www.weather.gov/media/ffc/ta_htindx.PDF.

Rowell, L. B., 1974: Human cardiovascular adjustments to exercise and thermal stress. *Physiological Reviews*, **54 (1)**, 75–159, https://doi.org/10.1152/physrev.1974.54.1.75.

Soto, K. I., 1982: Maximal sweating and sweating efficiency of acclimated men and women during work in the heat. Ph.D. thesis, 115 pp., URL https://www.proquest.com/docview/303238927.

Steadman, R. G., 1979: The assessment of sultriness. Part I: A temperature-humidity index based on human physiology and clothing science. *Journal of Applied Meteorology*, **18 (7)**, 861–873, https://doi.org/10.1175/1520-0450(1979)018⟨0861:TAOSPI⟩2.0.CO;2.

Taylor, C. L., 1957: Description and prediction of human response to aircraft thermal environments. *Transactions of the American Society of Mechanical Engineers*, **79 (5)**, 1024–1028.

Taylor, W. F., J. M. Johnson, D. O'Leary, and M. K. Park, 1984: Effect of high local temperature on reflex cutaneous vasodilation. *Journal of Applied Physiology*, **57 (1)**, 191–196.

Vanos, J., G. Guzman-Echavarria, J. W. Baldwin, C. Bongers, K. L. Ebi, and O. Jay, 2023: A physiological approach for assessing human survivability and liveability to heat in a changing climate. *Nature Communications*, **14 (1)**, 7653.

Vecellio, D. J., S. T. Wolf, R. M. Cottle, and W. L. Kenney, 2022: Evaluating the 35c wet-bulb temperature adaptability threshold for young, healthy subjects (psu heat project). *Journal of Applied Physiology*, **132**, 340–345, https://doi.org/10.1152/japplphysiol.00738.2021.

Webb, P., 1959: Human thermal tolerance and protective clothing. *Annals of the New York Academy of Sciences*, **82 (3)**, 714–723.

Webb, P., 1975: Thermal exchanges and temperature stress. *Foundations of Space Biology and Medicine: Ecological and Physiological Bases of Space Biology and Medicine*, M. Calvin, and O. G. Gazenko, Eds., Vol. II, Scientific and Technical Information Office, National Aeronautics and Space Administration, Washington, D.C., 94–126.

Wolf, S. T., R. M. Cottle, D. J. Vecellio, and W. L. Kenney, 2022: Critical environmental limits for young, healthy adults (PSU HEAT Project). *Journal of Applied Physiology*, **132 (2)**, 327–333.